Albertian errors in head-mounted displays: I. Choice of eye-point location for a near- or far-field task visualization

Jannick Rolland

School of Optics/CREOL/FPCE, University of Central Florida, Orlando, Florida 32816

Yonggang Ha

School of Optics/CREOL/FPCE, University of Central Florida, Orlando, Florida 32816

Cali Fidopiastis

Institute for Simulation and Training, University of Central Florida, Orlando, Florida 32816

Received December 4, 2003; revised manuscript received February 4, 2004; accepted February 9, 2004

A theoretical investigation of rendered depth and angular errors, or Albertian errors, linked to natural eye movements in binocular head-mounted displays (HMDs) is presented for three possible eye-point locations: the center of the entrance pupil, the nodal point, and the center of rotation of the eye. A numerical quantification was conducted for both the pupil and the center of rotation of the eye under the assumption that the user will operate solely in either the near field under an associated instrumentation setting or the far field under a different setting. Under these conditions, the eyes are taken to gaze in the plane of the stereoscopic images. Across conditions, results show that the center of the entrance pupil minimizes rendered angular errors, while the center of rotation minimizes rendered position errors. Significantly, this investigation quantifies that under proper setting of the HMD and correct choice of the eye points, rendered depth and angular errors can be brought to be either negligible or within specification of even the most stringent applications in performance of tasks in either the near field or the far field.

OCIS code: 330.1400.

1. INTRODUCTION

In today's information-intensive environment, some contexts require that three-dimensional data be rendered accurately and that remaining errors be quantified. The military, for example, is interested in the development of head-mounted displays (HMDs) that can accurately display information to increase visual awareness for detection, identification, and tracking of objects of interest, reduce cognitive demand, and improve navigation maneuvers. The medical and biomedical fields face similar challenges and require high-end technology for teaching, training, and guided surgery. For these high-demand applications, rendered objects may need to be localized within fractions of a degree and within millimeters.[1]

The mapping technique used to create two-dimensional (2D) stereoscopic images in HMDs is based on the principle of Alberti's window,[2] which first requires that the virtual cameras serving as equivalent eyes in the computer be reduced to single fixed points. Such points are referred to as eye points in the computer graphics and optics literature.[3,4] Furthermore, the mapping technique requires that the 2D planes on which three-dimensional (3D) virtual objects are mapped be not only level with the cameras but also perpendicular to the visual lines of the cameras for a straight-ahead direction (i.e., a visual line is defined as a line passing through both the pupil center and the nodal point).[5] Because current HMDs do not have eye-tracking capability, a "best" fixed eye point set in the software must be chosen for rendering stereoscopic images, where "best" is defined as an eye point that minimizes depth or angular errors in object space where the stimuli are defined according to a set of task requirements. The point located at the crossing of rays joining the eye points and the mapping points in the 2D stereoscopic images is referred to as **P** in this paper.

The fixed-eye-points assumption used for mapping stereoscopic images to a 3D object was highlighted as a possible cause of rendered depth errors in virtual environments.[6,7] It is well known that in real and virtual environments the eyes rotate toward the location of a 3D object of interest in order to avoid diplopic images.[8] As the eyes rotate, the centers of the entrance pupils move accordingly. Thus, if we consider fixed locations of the eye points for rendering images, the rays used to render a point in the virtual environment do not generally coincide with the dynamic chief rays, defined as the chief rays associated with natural eye movements, and thus natural motion of the pupil location. The dynamic chief rays play an important role in the apparent rendered point in object space for the HMD user, as further detailed below. Consequently, rendered depth and angular errors will generally occur as a result of where a point is appar-

1084-7529/2004/060901-12$15.00

ently rendered with respect to the dynamic pupils as opposed to where it is rendered with respect to the chosen eye points. These errors are related to the loss of alignment with the motion of the eye, also referred to as ocular parallax by Brewster.[9] Let us consider one eye and two objects positioned along the visual line.[5] Ocular parallax is then the phenomena of misalignment of the two objects that occurs with eye rotations. The reason for ocular parallax is that the pupil is not collocated with the center of rotation of the eye. Regarding two eyes in binocular vision, rendered depth error depends on the change in interpupillary distance (IPD) as well as the precise location of the eyes with respect to the rendered object. Angular errors depend on ocular parallax. These types of errors combined within Alberti's window paradigm, which we are using in computer graphics to render objects in virtual environments, were referred to in previous research as Albertian errors.[10]

To map stereoscopic images to three-dimensional objects in a HMD with no eye-tracking capability, three choices for the eye points' locations have been used: the entrance pupils, the nodal points, and the centers of rotation of the virtual cameras. Furthermore, it is suggested that once the stereoscopic images are rendered, both the nodal points and the entrance pupils of the eyes, which move as the eyes move establish the visual direction of the 3D point corresponding to the generated images. We shall now discuss why the pupils, as opposed to the nodal points, should be chosen to establish visual direction. This choice was first supported by Ogle's assertion that the chief rays (i.e., by definition the rays passing through the centers of the entrance pupils of the eyes), instead of the visual axis passing through the nodal points, should be used to determine the location of a rendered point in stereoscopic devices.[11,12] Rolland (1994) also stressed such a property as it applies to HMDs.[13] The Ogle assertion builds on the fact that Ogle recognized that the nodal points are only mathematical constructs out of the collineation framework for rotationally symmetric systems under the paraxial approximation.[11–14] While one of the important properties of a nodal ray is its unit angular magnification and its first-order achromatic property,[15] eyes have been shown to suffer from lateral chromatic aberrations in addition to axial chromatic aberrations because the pupil of the eye is not located at the nodal point of the eye. Such a finding further indicates that the pupils serve to establish visual direction. In some experiments Ye *et al.* decentered an artificial pupil to coincide with the visual axis,[15] which is optically equivalent to forcing the nodal ray to also be the chief ray. In doing so, Ye *et al.* could quantify the amount of lateral chromatic aberrations as a function of the amount of decentering of an artifical pupil with respect to the visual axis. In the case of natural pupils, the separation of the pupils from the nodal points is small, on the order of 4 mm; thus the pupils are closely aligned with the visual axes, and the lateral chromatic aberrations are small.[16] The fact that lateral chromatic aberrations are nonzero in the real world further indicates that the chief rays set visual direction.

Significantly, the centroid of the light impinging on the retina from any point in the field of view (FOV) is given by the chief ray for both in-focus and out-of-focus images under the assumption that the pupil is small enough for the coma aberration of the eye to be negligible. Thus the chief ray can be thought of as the axis of the pencil of rays, which actually enters the eye and stimulates the retina. While the nodal ray's impact on the retina coincides with the chief impact on the retina for in-focus images, such points of impact do not typically coincide for out-of-focus images. In some cases, the nodal ray may not even be part of the pencil of rays that stimulate the retina. Finally, the assertion that the chief ray should be considered to establish visual direction was validated experimentally in ophthalmology by studying nonemmetropic eyes.[17] For larger pupils when coma could play a role in displacing the chief ray impact from the centroid of retinal stimulation, the Stiles–Crawford effect has been shown to apodize the pupil to reduce such displacement in apparent visual direction.[18] Thus in this paper, given a point rendered as two 2D stereoscopic images, we set the rendered position of the point in 3D object space at the intersection of the two chief rays passing through the 2D rendered stereoscopic points.

We now return to the choice of the eye points in rendering the 2D stereoscopic images. The pupil is commonly chosen in the optics and ophthalmologic literature because it sets visual direction in object space. In spite of that, the nodal points have been extensively used in the stereoscopic vision and computer graphics literature because of their unit angular magnification, which allows the mapping of angular space one to one between object and retinal space.[19] In fact, such a choice may be explained in part by the fact that for in-focus imaging, whether a point in space is chosen at the intersection of the nodal rays or the chief rays makes no difference. It is only for out-of-focus images that the use of the nodal ray fails to predict correctly the location of a point in space from the centroid of energy on the retina.

Finally, it has also been suggested in the literature on visual instrumentation that the centers of rotation of the eyes instead of the centers of the entrance pupils be considered as the eye points.[20] Indeed as the eyes rotates, the pupil of each eye lines up with the corresponding center of rotation, and therefore the point rendered at the gaze location coincides precisely with the corresponding point on the virtual object. Thus the choice of the center of rotation as the eye point ensures that there is no rendered depth error at the gaze point in the computational model for stereo pair generation. This choice appears to solve the problem of having to dynamically adjust the eye points in software, a procedure that would require measuring eye movements. In light of this observation, it has been further suggested that selecting the centers of rotation of the eyes as the eye points could serve as an alternative to eye tracking in stereoscopic devices, if the requirement for eye tracking were intended to improve rendered depth accuracy.[6] Naturally, it is understood that many other motivations make eye tracking valuable in stereoscopic devices beyond the need for accuracy of rendered depth.[21–23] While small errors are expected in rendered depth around the gaze point if the center of rotation is chosen as the eye point, it is of interest to quantify their magnitude.[24] Furthermore, if angular errors are impor-

tant to an application, we must establish whether the center of rotation also yields minimum angular error.

In this paper, to establish visual direction we employ a model of image rendering based on the chief rays and thus on their intersection to localize an apparent rendered object point. We discuss the conditions under which such an intersection exists, as we theoretically demonstrate that the chief rays do not always intersect. We then quantify rendered errors by computing both the depth and the angular errors of the apparent rendered point from the dynamic pupils and the rendered point from the chosen fixed eye point. We consider the angles of elevation and azimuth suggested in the vision literature to parameterize the problem.[25] We take into account only the rotations of the eyes, neglecting the small translation motions during convergence. We also naturally consider HMDs without eye-tracking capability, given that in the contrary case we do know how to select the eye points at the pupil centers, under which condition rendering can be performed accurately.

This investigation provides a general mathematical framework to quantify Albertian errors in object space where rendering takes place, given various eye-point locations. We apply the framework by computing such errors for two eye points, the centers of rotation and the entrance pupils of the eyes, in both far- and near-field HMD configurations. We call near-field visualization the configuration for which the gaze point is located at arm's length (i.e., 1 m is chosen in the computation of errors). We call far-field visualization the configuration for which the gaze point is located farther than 6 m away from the user's eyes (i.e., 10 m is chosen in the computation of errors). In addition, we further assume that the HMD user is utilizing the display in either the near field or the far field. In either case, the microdisplay within the HMD is assumed to be positioned with respect to the focal point of the optics so that the stereoscopic images are presented at 1 m (i.e., for the near field), and 10 m (i.e., for the far field). For multiple-task requirements within a HMD that might occur sequentially in the near and the far field, the gaze point will not always lie in the plane of the stereoscopic images, and additional numerical assessments will be required.

2. METHODS

In order to quantify rendered depth and angular errors in HMDs, we shall first specify a computational framework with associated notation and definitions of errors in the rendered location of a point **P**. We shall then provide an expression for rendered errors and establish the conditions under which such errors can be computed.

A. Computational Framework

We shall denote any point in space as a bold letter to represent its vectorial form. Given a choice of eye point locations, let us denote as $\mathbf{V}_R^P$ the mapping point that corresponds to the mapping of a point **P** to the plane of the stereoscopic image for the right eye point. Similarly, the mapping point $\mathbf{V}_L^P$ may be obtained for the left eye point. By construction **P** lies at the intersection of the lines joining the eye points and the mapping points.

Given natural eye movements, when the mapping points $\mathbf{V}_L^P$ and $\mathbf{V}_R^P$ are joined via lines to the respective left and right dynamic pupils, the rendered point **P** is generally displaced to **P′**. The gaze point, denoted as $\mathbf{I}_g$, is also referred as the fixation point in the vision literature. However the term gaze point best represents a naturally moving eye, whereas the term fixation point best describes an eye fixating at one point in space in order to control some visual stimuli as commonly required in psychophysics. By construction, if the point **P** is located within the planes of the stereoscopic images, regardless of both the eye-point and the gaze-point locations, **P′** will be superimposed on **P**. In the case of 3D visualization where the points **P** are generally rendered within a volume, **P′** does not coincide with **P**.

In order to define some metrics for computing the magnitude of the rendered errors, we consider Fig. 1, where a frame of coordinates *X*, *Y*, and *Z* centered midway on the interocular axis at the point known as the cyclopean point **O** is considered. The interocular axis is taken to pass through the centers of rotation of the eyes, denoted as $\mathbf{C}_L$ and $\mathbf{C}_R$, for the left and right eyes, respectively. The interocular axis remains a still reference when the eyes rotate, which allows investigation of different eye points with a common fixed reference. The *XZ* plane is taken to be the horizon plane, which is also the transverse plane of the head. We define a horizontal (as opposed to vertical) plane of regard as the plane passing through the three points $\mathbf{C}_L$, $\mathbf{C}_R$, and $\mathbf{I}_g$. The binocular plane is defined as the plane passing through $\mathbf{C}_L$, $\mathbf{C}_R$, and the mapping points $\mathbf{V}_R^P$ and $\mathbf{V}_L^P$. Note that by construction of Alberti's windows, $\mathbf{C}_L\mathbf{C}_R$ is always parallel to $\mathbf{V}_R^P\mathbf{V}_L^P$, and these four points will always be coplanar. Let us denote the crossing point of $\mathbf{C}_L\mathbf{V}_L^P$ and $\mathbf{C}_R\mathbf{V}_R^P$ as **B**. If the centers of rotation of the eyes are chosen as eye points, **P** will be coincident with **B**. If the centers of the pupils are chosen as the eye points, the point **P** will be somewhere below the crossing point **B**. In Figs. 1 and 2, the centers of ro-

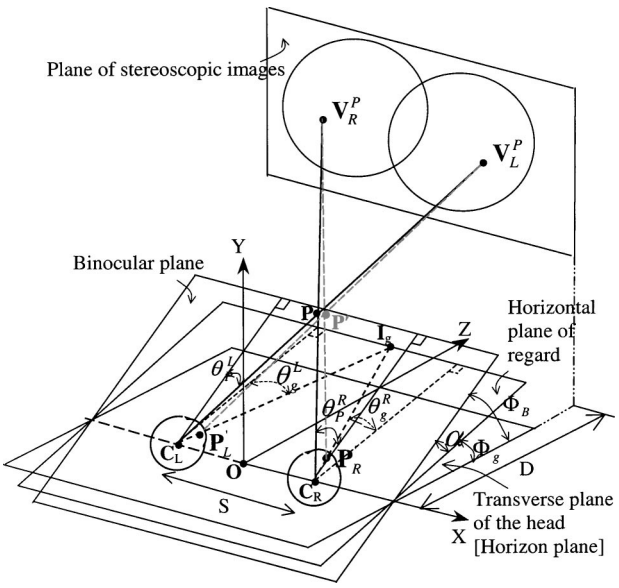

Fig. 1. Definition of the frame of coordinates. The centers of rotation of the eyes were chosen as the eye points for illustration purposes; point **B** (not shown) coincides with **P**.

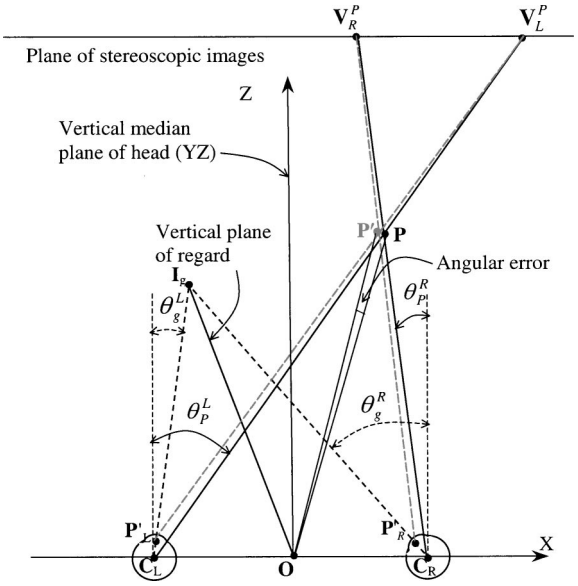

Fig. 2. Top view of the stereoscopic vision model presented in Fig. 1.

tation are chosen as the eye points for illustration, and the point **P** is shown (i.e., the point **B** is coincident with **P**, and for simplicity **B** is not represented in Figs. 1 and 2). Also because **B** is located in the binocular plane, it plays a key role in the derivation of the rendered errors.

The spatial coordinates of **B** will be expressed as a function of ϕ_B, the cyclopean elevation angle defined as the angle between the binocular plane and the horizon plane, and θ_B^L and θ_B^R are the azimuth angles in the binocular plane where L and R denote the angle with respect to the left and right eye points, respectively. Let us denote as α the oculocentric elevation angle defined as the angle between the plane of regard and the binocular plane and ϕ_g as the elevation angle between the horizon plane and the horizontal plane of regard. Similarly, the azimuth angles for the point $\mathbf{I}_g$ are denoted as θ_g^L and θ_g^R. We shall assume that the stereoscopic virtual images are displayed at a distance D from the interocular axis.

In the computations that follow, we investigate the rendered errors of a point **P** when the user gazes at $\mathbf{I}_g$. The coordinates of **P** are eye-point dependent and are given by the intersection of $\mathbf{E}^L\mathbf{V}_L^P$ and $\mathbf{E}^R\mathbf{V}_R^P$, where $\mathbf{E}^L$ and $\mathbf{E}^R$ denote the eye point's location for the left and the right eye, respectively. The eye points are considered to be either $\mathbf{C}_L$ and $\mathbf{C}_R$ or the centers of the left $\mathbf{P}_L$ and right $\mathbf{P}_R$ pupils for fixed straight-ahead gaze direction. Let us further denote as r the distance between the center of rotation of an eye and the corresponding eye point. Based on the two choices for eye-point location, r will be either zero or r_p for the center of rotation and the pupil, respectively. The convergence motion toward the gaze point $\mathbf{I}_g$ leads to a rotation of the eyes. Consequently as the eyeballs move, $\mathbf{P}_L$ and $\mathbf{P}_R$ rotate to their new locations $\mathbf{P}_L'$ and $\mathbf{P}_R'$, respectively. Thus the point **P** is displaced to $\mathbf{P}'$, which lies at the intersection of the dynamic chief rays $\mathbf{P}_L'\mathbf{V}_L^P$ and $\mathbf{P}_R'\mathbf{V}_R^P$.

We shall quantify the rendered angular error as the angular error for the cyclopean point **O**, given by

$$\mathrm{AngE} = \arccos\left(\frac{\mathbf{OP}\cdot\mathbf{OP}'}{\|\mathbf{OP}\|\cdot\|\mathbf{OP}'\|}\right), \tag{1}$$

where the function AngE depends implicitly on the parameters θ_B^L, θ_B^R, α, θ_g^L, θ_g^R, d, and D. Given the value of AngE, the rendered depth error corresponds to the displacement of **P** to $\mathbf{P}'$ computed in the horizontal plane of regard in millimeters and can then be expressed as

$$\mathrm{DepthE} = |z_P - z_{P'}|/\cos(\phi_g). \tag{2}$$

B. Expression of the Coordinates of the Point P'

The quantification of Albertian errors, which are created as a consequence of a discrepancy between the coordinates of **P** and $\mathbf{P}'$, requires that the coordinates of **P**, the centers of the rotated entrance pupils, and $\mathbf{P}'$ be expressed with respect to angular parameters.

1. Expression of the Coordinates of the Point P

Let us denote as S the separation between the centers of rotation $\mathbf{C}_L$ and $\mathbf{C}_R$. On the basis of trigonometry derivable in the binocular plane from Fig. 1, the coordinates of the mapping points $\mathbf{V}_L^P$ and $\mathbf{V}_R^P$ are respectively given by

$$\mathbf{V}_L^P\left(\frac{D\tan\theta_B^L}{\cos\phi_B} - \frac{S}{2},\, D\tan\phi_B,\, D\right),$$

$$\mathbf{V}_R^P\left(\frac{D\tan\theta_B^R}{\cos\phi_B} + \frac{S}{2},\, D\tan\phi_B,\, D\right). \tag{3}$$

The point **P** is located at the intersection of $\mathbf{E}^L\mathbf{V}_P^L$ and $\mathbf{E}^R\mathbf{V}_P^R$, and its coordinates satisfy the system of equations

$$\mathbf{E}^L\mathbf{P} = k_1\ \mathbf{E}^L\mathbf{V}_P^L,$$

$$\mathbf{E}^R\mathbf{P} = k_1'\ \mathbf{E}^R\mathbf{V}_P^R, \qquad (k_1, k_1') \in \Re^2. \tag{4}$$

Using the Thales theorem in the parallelogram $\mathbf{E}^L\mathbf{E}^R\mathbf{V}_P^L\mathbf{V}_P^R$, we establish that k_1 and k_1' are given by

$$k_1 = k_1' = \frac{S\cos(\phi_B)}{D(\tan\theta_B^L - \tan\theta_B^R)}. \tag{5}$$

Substituting for k_1 and k_1' in Eqs. (4) yields the coordinates of **P** given by

$$x_P = \frac{S}{2} + \frac{S\tan\theta_B^R}{(\tan\theta_B^L - \tan\theta_B^R)},$$

$$y_P = \frac{S\sin\phi_B}{(\tan\theta_B^L - \tan\theta_B^R)},$$

$$z_P = r + \frac{S\cos\phi_B}{D(\tan\theta_B^L - \tan\theta_B^R)}(D - r). \tag{6}$$

If we substitute x_p, y_p, and z_p given in Eqs. (6) for θ_B^L, θ_B^R, and ϕ_B given in Eqs. (3), the coordinates of the mapping points $\mathbf{V}_L^P$ and $\mathbf{V}_R^P$ can be expressed as

$$\mathbf{V}_L^P\left(\frac{(D-r)(x_p+S/2)}{z_p-r}-\frac{S}{2},\frac{(D-r)y_p}{z_p-r},D\right),$$

$$\mathbf{V}_R^P\left(\frac{(D-r)(x_p-S/2)}{z_p-r}+\frac{S}{2},\frac{(D-r)y_p}{z_p-r},D\right). \quad (7)$$

In the case when z_p given in Eqs. (7) equals D, the coordinates of the mapping points $\mathbf{V}_L^P$ and $\mathbf{V}_R^P$ will merge into one point at (x_p, y_p, D) that superimposes precisely on $\mathbf{P}$ as previously described. Such a condition will naturally not be affected by the choice of the eye point.

2. Expression of the Coordinates of the Centers of the Rotated Entrance Pupils

The location of the centers of the entrance pupil during gazing in object space is fundamental to the computation of errors since the chief rays are used to establish the visual directions of a point. The centers of the entrance pupils do not remain still because of the natural convergence motion of the eyes, which can be described as a composition of two successive rotations θ_g^L and ϕ_g and θ_g^R and ϕ_g for the left and the right eye, respectively. The centers of the entrance pupils then rotate from the horizon plane to the plane of regard by these rotations. The coordinates of the rotated center of the entrance pupil $\mathbf{P}_L'$ for the left eye are therefore

$$\mathbf{OP}_L'\begin{pmatrix} r_P\sin\theta_g^L - S/2 \\ r_P\cos\theta_g^L\sin\phi_g \\ r_P\cos\theta_g^L\cos\phi_g \end{pmatrix}. \quad (8)$$

Similarly, the coordinates of the rotated center of the entrance pupil $\mathbf{P}_R'$ for the right eye are

$$\mathbf{OP}_R'\begin{pmatrix} r_P\sin\theta_g^R + S/2 \\ r_P\cos\theta_g^R\sin\phi_g \\ r_P\cos\theta_g^R\cos\phi_g \end{pmatrix}. \quad (9)$$

3. Expression of the Coordinates of the Point $\boldsymbol{P}'$

Provided the expressions for the coordinates of $\mathbf{P}$ as well as the centers of the rotated entrance pupils, $\mathbf{P}'$ is located at the intersection of $\mathbf{P}_L'\mathbf{V}_L^P$ and $\mathbf{P}_R'\mathbf{V}_R^P$. Its coordinates are then the solution of the system of equations

$$\mathbf{P}_L'\mathbf{P}' = k_2\ \mathbf{P}_L'\mathbf{V}_L^P,$$

$$\mathbf{P}_R'\mathbf{P}' = k_2'\ \mathbf{P}_R'\mathbf{V}_R^P, \qquad (k_2, k_2') \in \Re^2. \quad (10)$$

By matching the x_P' and z_P' expressions in Eqs. (10), one finds that the coefficients k_2 and k_2' satisfy the system

$$\begin{pmatrix} c \\ d \end{pmatrix} = \mathbf{M}\begin{pmatrix} k_2 \\ k_2' \end{pmatrix} = \begin{bmatrix} a & b \\ a' & b' \end{bmatrix}\begin{pmatrix} k_2 \\ k_2' \end{pmatrix}, \quad (11)$$

where

$$c = r_P(\sin\theta_g^R - \sin\theta_g^L) + S,$$

$$a = \frac{D\tan\theta_B^L}{\cos\phi_B} - r_P\sin\theta_g^L,$$

$$b = -\left(\frac{D\tan\theta_B^R}{\cos\phi_B} - r_P\sin\theta_g^R\right),$$

$$d = r_P\cos\phi_g(\cos\theta_g^R - \cos\theta_g^L),$$

$$a' = D - r_P\cos\theta_g^L\cos\phi_g,$$

$$b' = -(D - r_P\cos\theta_g^R\cos\phi_g). \quad (12)$$

The expressions for k_2 and k_2' are thus given by

$$k_2 = \frac{b'c - db}{\det(\mathbf{M})},$$

$$k_2' = \frac{ad - ca'}{\det(\mathbf{M})}. \quad (13)$$

We then obtain the coordinates of $\mathbf{P}'$ as a function of the azimuth and elevation angles of $\mathbf{P}$ and $\mathbf{I}_g$ by substituting in Eqs. (13) the expression for k_2' given in Eqs. (10). To give more insight into the numerical applications, it is possible to replace ϕ_B by $(\phi_g + \alpha)$ to express the coordinates of $\mathbf{P}'$ as a function of α. The coordinates of $\mathbf{P}'$ are then given by

$$x_{P'} = r_P\sin\theta_g^R + \frac{S}{2} + k_2'\left(\frac{D\tan\theta_g^R}{\cos(\phi_g+\alpha)} - r_P\sin\theta_g^R\right),$$

$$y_{P'} = r_P\cos\theta_g^R\sin\phi_g + k_2'((D\tan(\phi_g+\alpha) - r_P\cos\theta_g^R\sin\phi_g),$$

$$z_{P'} = r_P\cos\theta_g^R\cos\phi_g + k_2'(D - r_P\cos\theta_g^R\cos\phi_g). \quad (14)$$

The expression for the coordinates of $\mathbf{P}'$ exists under the assumption that the chief rays intersect. The existence of such an intersection in three-dimensional space is now discussed.

C. Conditions for an Intersection of Chief Rays in Three-Dimensional Space

In a three-dimensional virtual environment, the location of $\mathbf{P}'$ may be derived only if the chief rays passing through the pupils centers intersect. This condition requires that $\mathbf{P}_L'\mathbf{P}_R'$ and $\mathbf{V}_L^P\mathbf{V}_R^P$ be coplanar. Furthermore we may distinguish between two cases: case 1, where $\mathbf{P}_L'\mathbf{P}_R'$ is not parallel to $\mathbf{V}_L^P\mathbf{V}_R^P$, in which case the intersection of the rays requires that $\mathbf{V}_L^P\mathbf{V}_R^P$ lie in the plane of regard, and case 2, where $\mathbf{P}_L'\mathbf{P}_R'$ is parallel to $\mathbf{V}_L^P\mathbf{V}_R^P$, in which case the gaze point is consequently in the vertical median plane of the head.

1. Case 1: $\mathbf{V}_L^P$ and $\mathbf{V}_R^P$ are in the Plane of Regard

If $\mathbf{V}_L^P$ and $\mathbf{V}_R^P$ lie in the plane of regard, because by definition $\mathbf{P}_L'$ and $\mathbf{P}_R'$ are in the plane of regard, then $\mathbf{P}$ necessarily lies in the plane of regard, and α equals zero. In this case, $\phi_g = \phi_B$ and there is an intersection of the chief rays for any location of the gaze point in this plane. The point $\mathbf{P}'$ is then rendered in the plane of regard.

2. Case 2: $\mathbf{V}_L^P$ and $\mathbf{V}_R^P$ are Not in the Plane of Regard

If $\mathbf{V}_L^P$ and $\mathbf{V}_R^P$ are not included in the plane of regard, the chief rays' intersection exists if and only if $\mathbf{P}_L'\mathbf{P}_R'$ is parallel to $\mathbf{V}_L^P\mathbf{V}_R^P$. Since $\mathbf{C}_L\mathbf{C}_R$ is parallel to $\mathbf{V}_L^P\mathbf{V}_R^P$ by definition of the mapping points, the vectors $\mathbf{P}_L'\mathbf{P}_R'$ and $\mathbf{V}_L^P\mathbf{V}_R^P$ are then parallel if $\mathbf{P}_L'\mathbf{P}_R' \times \mathbf{C}_L\mathbf{C}_R = 0$, where $\times$ denotes the cross product of two vectors. This condition leads to

$|\theta_g^L| = |\theta_g^R|$. The solution $\theta_g^L = \theta_g^R$ leads to $\mathbf{P}'_L\mathbf{C}_L$ parallel to $\mathbf{P}'_R\mathbf{C}_R$, which means that the eyes are gazing at infinity and at any angle. This case is sensible only for far-field visualization with a collimated display, in which case there will be no error in rendered depth given that the plane of the stereoscopic images will be at infinity as well. Therefore the only solution we need to consider is the case where the plane $x = 0$ is the only solution for the gaze point, which corresponds to the vertical median plane of the head. It is important to note that if the chief rays do not intersect, the location of the point $\mathbf{P}'$ cannot be derived as the simple intersection of two rays. Such a finding is discovered through this analysis because we do not make the simple assumption that an eye can be reduced to a single static point through which all projections are computed.

3. RESULTS

In order to compute the magnitude of the errors provided by Eqs. (1) and (2), we must first choose reasonable values of the HMD field of view and observation parameters. Results will be presented according to the two possible cases of getting an intersection of the chief rays as defined in Section 2. For each case of intersection presented, angular errors for the far-field and near-field HMD configurations will be quantified separately. In the near-field case, depth errors will also be quantified. The need to investigate separately near- and far-field visualization stems from the current limitation of the HMD optics, which simply present the stereoscopic images at a fixed distance D from the users' eyes. In this specific investigation, without loss of generality in the overall condition, we shall choose the values of D as 1 and 10 m for near field and far field, respectively. In quantifying the errors, we shall compare the magnitude of the angular errors with visual acuity up to eccentricities of 25 deg, which corresponds to half the diagonal FOV considered. Depth errors will be provided both in millimeters, which provides a practical feeling for the magnitude of the errors, and in arcseconds in order to relate them to human stereoacuity.

Table 1. Simulation Parameters

Parameter	Near-Field Visualization	Far-Field Visualization
D (m)	1	10
z_g (m)	1	10
Rendering depth z_p (m)	0.73 ~ 1.32	5.08 ~ 329.0
Vertical FOV ϕ_g, ϕ_B (°)	±15	
Horizontal FOV θ_g^L, θ_B^L (°)	±20	
r_p (mm)	9.25	

The variable z_p, which is the z coordinate of $\mathbf{P}$, is varied for the far-field case according to the depth of field around the value z_g (i.e., 10 m), the z coordinate of $\mathbf{I}_g$, which ranges from 5.08 to 329.0 m. For the near-field case, because the depth of field around 1 m varies only from 0.73 to 1.32 m but it is common in HMDs to render large objects in the near field of visualization, z_p is varied three times the range on either side of 1 m.[26] Such configurations allow for typical visualization scenarios in HMDs, where different settings are chosen for different applications. For example, visualization of collimated targets in military cockpits is a possible application of a far-field configuration, and near-field visualization may be used in medical visualization to superimpose data on a patient's body for guided surgery.

To quantify the numerical data of an average human eye, we employed the numerical features of the schematic eye proposed by Gullstrand.[10] While many other models have been proposed for various investigations related to the aberrations and physiology of the human eye, the only parameter we need to consider in this investigation is r_p (i.e., the distance between the pupil eye point and the center of rotation of the eye). Thus any model is appropriate because all models lead to the same value of that parameter within approximately ±1 mm. A quantification of the effect of such variation on errors will be presented below. The entrance pupil is the image of the iris through the refracting surface of the cornea. With this model, the distance between the center of the entrance pupil and the vertex of the cornea is computed to be 3 mm. The distance between the center of rotation and the vertex of the cornea is 12.25 mm. Thus the parameter r_P is taken to be 9.25 mm. The IPD distance is taken to be 65 mm to provide an estimate of the Albertian errors for an average IPD distance. The model of the eye does not take into account Listing's law or ocular kinematics given that we are restricting the investigation to object space. Consequently, we consider an approximation to the center of ro-

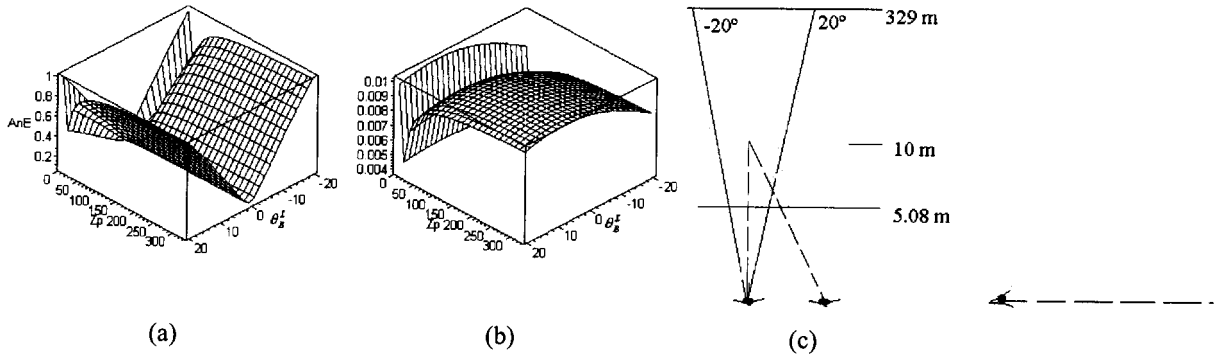

Fig. 3. Angular errors for $\theta_g^L = 0°$ and $\phi_g = 0°$, case 1, far field. Angular errors (a) when the centers of rotation of the eyes are taken as the eye points and (b) when the centers of pupils of the eyes are taken as the eye points. (c) Top and side views of the observation direction of the eyes.

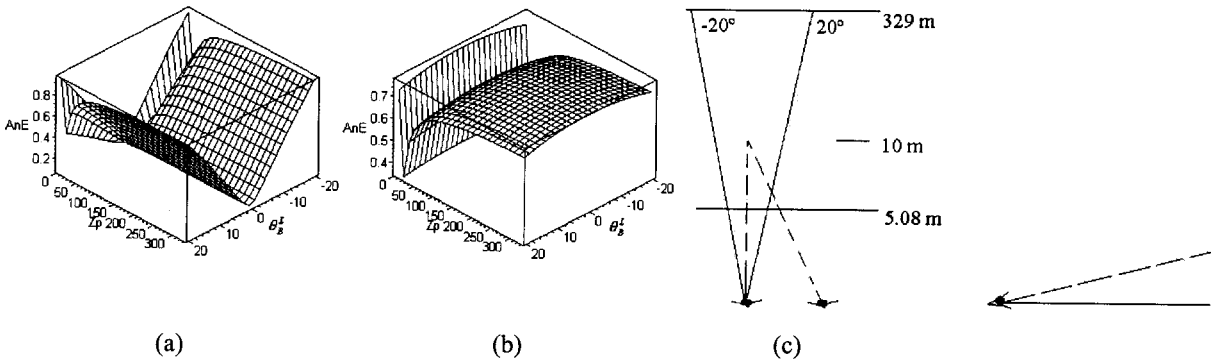

Fig. 4. Angular errors for $\theta_g^L = 0°$ and $\phi_g = 15°$, case 1, far field; (a)–(c) as in Fig. 3.

Table 2. Angular Errors as θ_g^L and ϕ_g Vary for Case 1, Far Field, for $D=10$, $z_g=10$, $\alpha=0$

		Maximum Magnitude of Angular Error (arc min)		Condition When Angular Error Reaches Minimum	
θ_g^L (°)	ϕ_g (°)	$\mathbf{C}_L$ and $\mathbf{C}_R$ as Eye Points	$\mathbf{P}_L$ and $\mathbf{P}_R$ as Eye Points	$\mathbf{C}_L$ and $\mathbf{C}_R$ as Eye Points	$\mathbf{P}_L$ and $\mathbf{P}_R$ as Eye Points
0	0	1	0.01	$\theta_B^L = 0$ or $z_p = 10$	$z_p = 10$
0	15	0.8	0.7		
10	0	1.4	0.5	$\theta_B^L = 10$ or $z_p = 10$	
10	15	1.4	0.9		
−10	0	1.4	0.5	$\theta_B^L = -10$ or $z_p = 10$	
−10	15	1.4	0.9		
20	0	2.0	1.1	$\theta_B^L = 20$ or $z_p = 10$	
20	15	2.0	1.3		
−20	0	2.0	1.1	$\theta_B^L = -20$ or $z_p = 10$	
−20	15	2.0	1.3		

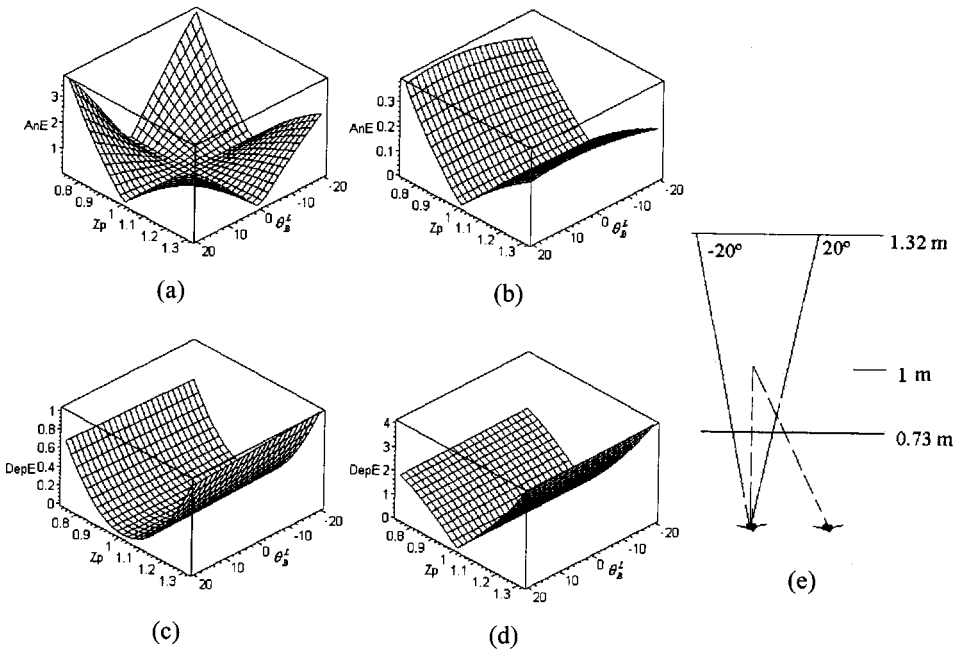

Fig. 5. Angular errors for $\theta_g^L = 0°$ and $\phi_g = 0°$, case 1, near field. Angular errors (a) when the centers of rotation of the eyes are taken as the eye points and (b) when the centers of pupils of the eyes are taken as the eye points. Depth errors (c) with centers of rotation of the eyes as the eye points and (d) with centers of pupils of eyes as the eye points. (e) Top and side views of the observation direction of the eyes.

tation as a unique point, which is required for the Alberti framework.

For the FOV of the observation conditions, both θ_g^L and θ_B^L were chosen to be ± 20 deg according to natural eye motion within ± 20 deg from a straight-ahead gazing position and in accordance with a horizontal FOV of 40 deg imposed, for example, by a microdisplay size and associated magnifying optics. Beyond such angles, users of head-mounted displays would naturally turn their heads to look at a point located farther in the FOV. The variables ϕ_g and ϕ_B will consequently define the vertical angle of the gaze point and the vertical FOV of observation, respectively. In this investigation, these two variables are limited to a maximum value of ± 15 deg given a vertical FOV of 30 deg assuming a microdisplay of 4:3 aspect ratio. Given that α is the difference between ϕ_g and ϕ_B, ϕ_g and α are varied in the simulations so the modulus of ϕ_g plus α does not exceed 15 deg. The simulation parameters are summarized in Table 1.

We shall now detail the computation of Albertian errors in the two cases of intersection of the chief rays. In the first case, for both the far-field and the near-field analysis, angular errors are plotted as a function of θ_B^L and z_p for different gaze-point locations θ_g^L and ϕ_g. The variables

Table 3. Angular and Depth Errors as θ_g^L and ϕ_g Vary for Case 1, Near Field, for $D=1$, $z_g=1$, $\alpha=0$

		Maximum Magnitude of Angular Error (arc min)		Maximum Magnitude of Depth Error (mm)	
θ_g^L (°)	ϕ_g (°)	$\mathbf{C}_L$ and $\mathbf{C}_R$ as Eye Points	$\mathbf{P}_L$ and $\mathbf{P}_R$ as Eye Points	$\mathbf{C}_L$ and $\mathbf{C}_R$ as Eye Points	$\mathbf{P}_L$ and $\mathbf{P}_R$ as Eye Points
0	0	4	0.4	1	4.2
0	15	4	3	0.8	4.2
10	0	5.4	1.7	1.1	4.2
10	15	5.4	3.4	1.0	4.2
−10	0	5.4	3.0	1.1	4.2
−10	15	5.4	4.0	1.0	4.2
20	0	7.2	4.0	1.0	4.2
20	15	7.2	5.0	1.0	4.2
−20	0	7.2	4.4	1.2	4.2
−20	15	7.2	5.0	1.0	4.2

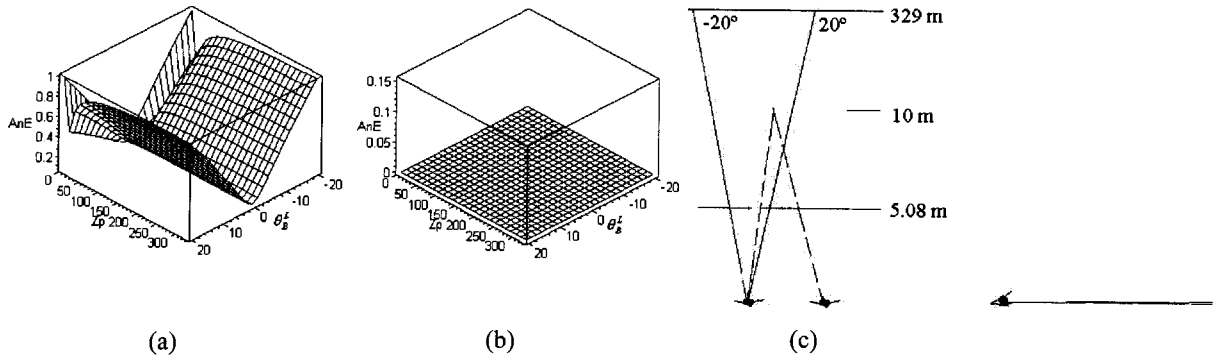

Fig. 6. Angular errors for $\alpha = 0°$ and $\phi_g = 0°$, case 2, far field; (a)–(c) as in Fig. 3.

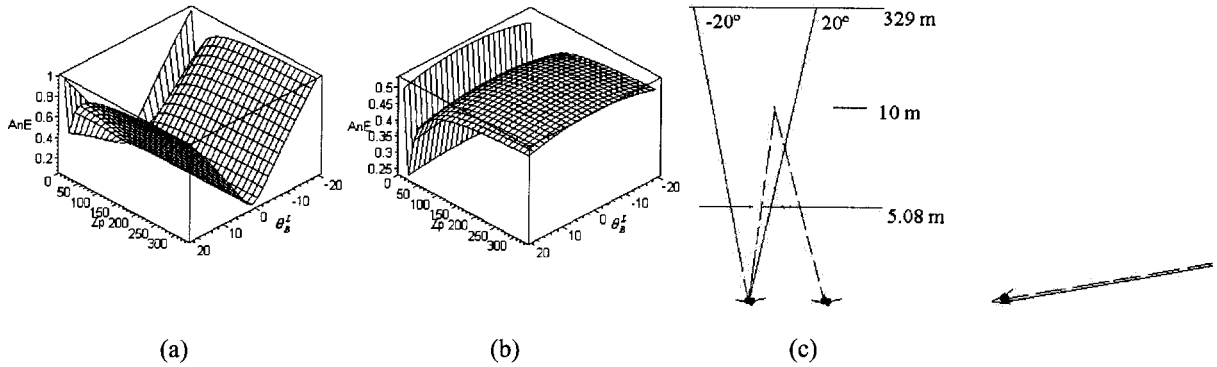

Fig. 7. Angular errors for $\alpha = 0°$ and $\phi_g = 10°$, case 2, far field; (a)–(c) as in Fig. 3.

Table 4. Angular Errors as ϕ_g and α Vary for Case 2, Far Field, for $D=10$, $z_g=10$, $\theta_g^L=-\theta_g^R$

		Maximum Magnitude of Angular Error (arc min)		Condition When Angular Error Reaches Minimum	
ϕ_g (°)	α (°)	$\mathbf{C}_L$ and $\mathbf{C}_R$ as Eye Points	$\mathbf{P}_L$ and $\mathbf{P}_R$ as Eye Points	$\mathbf{C}_L$ and $\mathbf{C}_R$ as Eye Points	$\mathbf{P}_L$ and $\mathbf{P}_R$ as Eye Points
0	−15	1.2	0.024		
0	−10	1.2	0.016		
0	−5	1.2	0.008		
0	0	1.2	0		
10	−25	1.5	0.5		
10	−10	1.1	0.54	$z_p = 10$	$z_p = 10$
10	0	1	0.53		
10	5	1	0.52		
15	−30	1.6	0.75		
15	−20	1.4	0.8		
15	−10	1.2	0.8		
15	0	1.0	0.78		

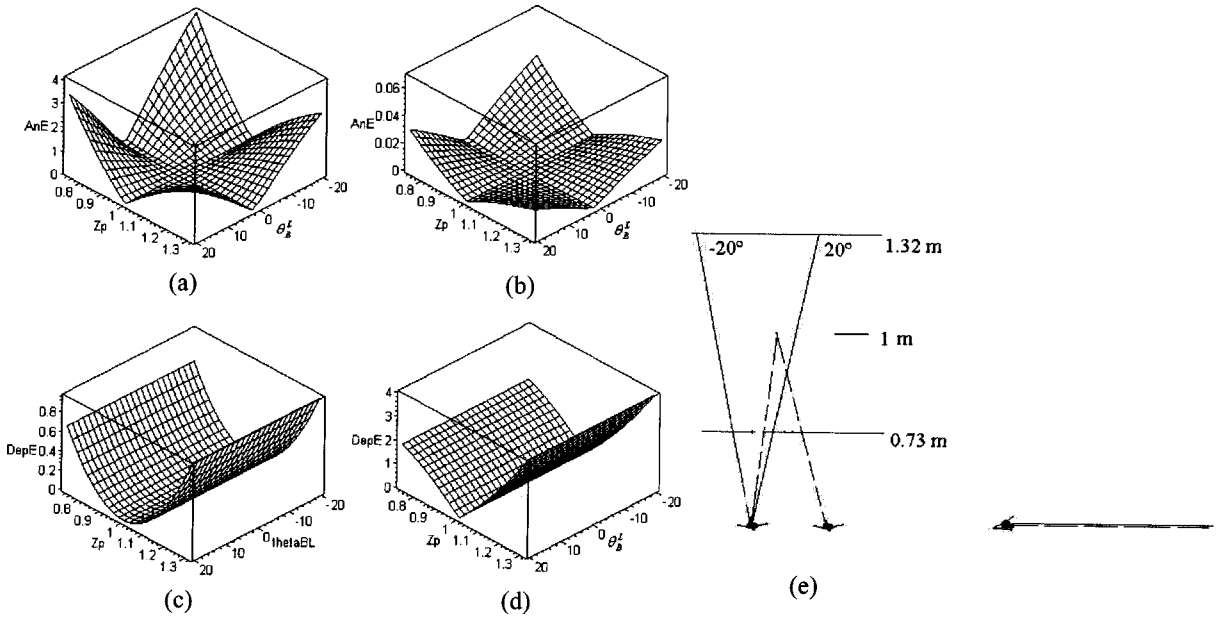

Fig. 8. Angular errors for $\alpha = 0°$ and $\phi_g = 0°$, case 2, near field; (a)–(e) as in Fig. 5.

z_p and θ_g^L in the figures are expressed in meters and degrees, respectively, and angular and depth errors are expressed in arc minutes and millimeters, respectively. For near-field analysis, depth errors are also plotted as a function of z_p and θ_B^L, for various pair values of θ_g^L and ϕ_g. Figures 3 and 4 show the angular errors for the far field for $\theta_g^L = 0°$ and $\phi_g = 0°$ and for $\theta_g^L = 0°$ and $\phi_g = 15°$, respectively, for two different eye points—the centers of rotation of the eyes and the centers of the entrance pupils. Table 2 shows angular errors as θ_g^L and ϕ_g vary. Figure 5 shows the angular and depth errors in the near field for $\theta_g^L = 0°$ and $\phi_g = 0°$ for two different eye points. Table 3 shows angular and depth errors as θ_g^L and ϕ_g vary.

In the second case of chief-ray intersection, where the gaze point is fixed in the median vertical plane of the head, angular errors are plotted as a function of θ_B^L and z_p with different values of α and ϕ_g for both the near and the far fields. Depth errors are plotted only for the near field as we have done for case 1. Figure 6 shows the angular errors in the far field for $\alpha = 0°$ and $\phi_g = 0°$ for two different eye points. Figure 7 shows the angular errors in the far field for $\alpha = 0°$ and $\phi_g = 10°$. Table 4 shows the angular errors as θ_g^L and ϕ_g vary. Figure 8 shows the angular and depth errors in the near field for $\theta_g^L = 0°$ and $\phi_g = 0°$ for two different eye points. Figure 9 shows the angular and depth errors in the near field for $\theta_g^L = 0°$ and $\phi_g = 10°$. Table 5 shows the angular and depth errors as θ_g^L and ϕ_g vary.

4. DISCUSSION

Considering the first case presented and far-field visualization, results presented in Fig. 3(b) show that the angular error is negligible (i.e., ~0.01 arc min) for the pupil as the eye point. Figure 3(a), which corresponds to the cen-

ter of rotation displays only slightly higher angular errors up to 1 arc min at the edge of the FOV. These results correspond to a zero gaze-point elevation angle (i.e., $\phi_g = 0$). In the case of nonzero elevation angle (i.e., $\phi_g = 15$ deg), Fig. 4 shows that the angular errors for the center of rotation have approximately the same value, whereas the angular errors for the pupil as the eye point increase to ~0.7 arc min. Table 2 shows that for the worst-case scenario of the eyes gazing at the corner of the display, the angular errors are 1.3 arc min for the pupil and increase to 2 arc min for the center of rotation. If interpreted in the context of the visual acuity of the human system, such angular errors are negligible if we consider ~1 arc min visual acuity within the fovea and an exponential decrease from that value up to ~10 arc min at 25 deg FOV.[27] Table 2 further shows that the minimum errors are zero for both the pupil and the center of rotation, which occur when the rendered point is located in the plane of the stereoscopic images, as expected. Another case of zero error, as expected is found for the center of rotation as the eye point when $\theta_g^L = \theta_B^L$, given that the rotated pupils are along the chief rays in this case. Such cases validate the expression derived in the mathematical framework. Although errors may become larger with larger FOVs, in practice, it is expected that beyond the 40×30 degree FOV, users will rotate their heads to look at a target. Results thus suggest that in far field, while the pupil theoretically leads to minimum angular errors if considered as the eye point, the center of rotation as the eye point yields maximum angular errors of only 2 arc min. Therefore, within a practical setting of ±25-deg diagonal FOV, all computed angular errors are within the

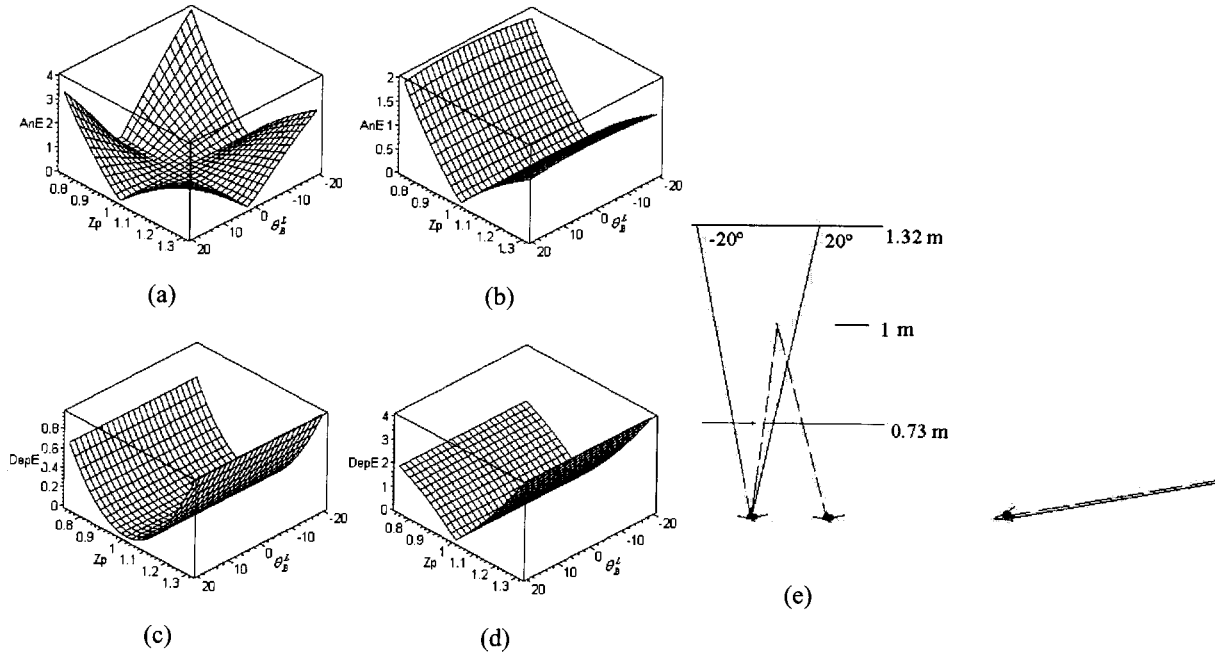

Fig. 9. Angular errors for $\alpha = 0°$ and $\phi_g = 10°$, case 2, near field; (a)–(e) as in Fig. 5.

Table 5. Angular and Depth Errors as ϕ_g and α Vary for Case 2, Near Field, for $D=1$, $z_g=1$, $\theta_g^L=-\theta_g^R$

		Maximum Magnitude of Angular Error (arc min)		Maximum Magnitude of Depth Error (mm)	
ϕ_g (°)	α (°)	$\mathbf{C}_L$ and $\mathbf{C}_R$ as Eye Points	$\mathbf{P}_L$ and $\mathbf{P}_R$ as Eye Points	$\mathbf{C}_L$ and $\mathbf{C}_R$ as Eye Points	$\mathbf{P}_L$ and $\mathbf{P}_R$ as Eye Points
0	−15	4.8	0.05	1.0	4.2
0	−10	4.4	0.04	1.0	4.2
0	−5	4.2	0.037	1.0	4.2
0	0	4.2	0.07	1.0	4.2
10	−25	5.6	2.0	1.0	4.2
10	−10	4.6	2.2	1.0	4.2
10	0	4.2	2.1	1.0	4.2
10	5	4.2	2.0	1.0	4.2
15	−30	6.4	2.8	1.0	4.2
15	−20	5.4	3.0	1.0	4.2
15	−10	4.6	3.0	1.0	4.2
15	0	4.0	2.9	1.0	4.2

visual acuity limit of the human visual system at the appropriate eccentricity where the point **P** was rendered, regardless of the choice of the eye point.

Now considering the first case presented and near-field visualization, results show that depth errors for the center of rotation as the eye point are of the order of 1 mm across conditions, as shown in Fig. 5(c) and Table 3, while depth errors reach 4.2 mm for the pupil as the eye point. From a theoretical point of view, depth errors of 1 mm for the eye gazing at 1-m distance while the rendered point **P** is displayed within the ±25 degrees field of view correspond to ~200 arc sec, which can be resolved within a few degrees of the gaze point (i.e., stereoacuity is less than 50 arc sec across variable stimuli conditions)[27] but cannot be resolved according to stereoacuity values for points in the field of view beyond at least 10 deg eccentricity.[5] In all cases, from a practical point of view, low eccentricity performance is most stringent and 1-mm depth error at 1 m is typically within the requirements for accurate rendering in HMDs, even for some of the most stringent applications such as augmented reality for medical procedures. Augmented reality refers to the optical superimposition of virtual models on real objects or scenes.[24,26] Concerning angular errors, results displayed in Figs. 5(a) and 5(b) as well as in Table 3 show that errors reach 7.2 arc min at the edge of the FOV, which is slightly above the 6-arc-min visual acuity of the human visual system at 25-deg eccentricity. Errors are found to be 5 arc min for the pupil at 25 deg in the FOV, which is within the visual acuity of the human visual system. Thus the pupil is the preferred point in the minimization of angular errors in the near-field case. If depth accuracy is most important, however, the center of rotation should be chosen as the eye point. Given the magnitude of the errors across conditions, if both depth and angular metrics are important, it is suggested that the center of rotation be used as the eye point.

For the second case presented and far-field visualization, results presented in Fig. 6, Fig. 7, and Table 4 show trends similar to those in the first case investigated, in that either the pupil or the center of rotation may be chosen as the eye point given the magnitude of the errors within the visual acuity of the human visual system. For the near-field visualization, a trend similar to that found in case 1 and shown in Fig. 8, Fig. 9, and Table 5 shows that the center of rotation is the preferred eye point for minimizing depth errors, whereas the pupil is preferred for minimizing angular errors. However, if both metrics are important, the center of rotation should be chosen as the eye point.

In summary, results show that while the pupil of the eye is theoretically superior as the eye point for far-field visualization, the center of rotation yields only slightly higher rendered angular errors, and thus either point may be chosen as the eye point with no consequences in practice. In the case of near-field visualization, the center of rotation should be chosen to minimize rendered depth errors, while the pupil is slightly superior in minimizing rendered angular errors. Thus, for either near or far field, given that the stereoscopic image planes were displayed differently according to these two cases, rendered angular error may be minimized by choosing the pupil as the eye point, whereas rendered depth error may be minimized by choosing the center of rotation as the eye point.

We now consider a few other observations. Results show that under near-field visualization, the depth errors as computed along the plane of regard given by Eq. (2), as opposed to simply along the Z axis, are constant on the order of 1 mm for the center of rotation as the eye point and 4.2 mm for the pupil for both cases 1 and 2. Furthermore, variation of the parameter r_p by ±1 mm to investigate the robustness of the results across various eye models leads to no significant increase in the errors reported (i.e., <10% across all conditions). It is important to note that this investigation treats the case of using the HMD in either a near-field or a far-field visualization, where the gaze point can thus be considered located within the plane of the stereoscopic images. In the case of dual use of near and far field for various tasks within the same application, the magnitude of the errors will increase significantly, and questions for future investigation are to establish whether there is a preferred location of the eye point under such dual-task scenarios, whether a restricted scope of tasks may be established under such visualization, and when is it that eye tracking becomes necessary for accurate depth and angular judgments. The framework presented in this paper is general and can be used to investigate such cases.

Before ending our discussion, we emphasize that the study presented here relates solely to object or rendered space, as opposed to visual space. When visual space is considered, special attention may be given to the optical aberrations of the eye and the associated issues of pupil location with respect to the visual axis, the pupil diameter, the corresponding retinal points, and the Stiles–Crawford effect, all of which play a role in perceptual judgments of visual direction and depth. The importance of such factors has been studied in the vision literature, and understanding their full significance in perception in HMDs, while beyond the scope of this paper, is of critical importance. In the experiments of Ye *et al.*[15] previously cited, for example, the pupil of the human eye was dilated, and an artificial pupil smaller than the eye pupil was located in front of the eye. Such a situation may occur in stereoscopic microscopes, as pointed out by the authors. In HMDs, it is important to note that it is the other way around: The pupil of the instrument under proper utilization is much larger than that of the eye (e.g., eye pupil 3–5 mm and instrument pupil 12–17 mm). Therefore, because the natural pupils are expected to be the limiting aperture in HMDs, chromostereopsis is negligible, for example, as is also found in the real world. However, proper utilization of a HMD device thus requires that IPD adjustment be available to ensure that the natural pupils always limit the pupil of the system. Another requirement is that the brightness of the display be such that the pupil of the eye will be small with respect to the pupil of the HMD. It is only in the case of systems designed with pupil sizes of less than 10 mm that issues of brightness could start playing a role in how the human pupil is located within the system pupil. Furthermore, the rendering software must account for the IPD from each user in order to render visual directions accurately in object space for that user. Thus characterization of

the stimulus presented in a HMD is only one important part of the problem of quantifying perceptual angular and depth errors. The system as a whole and how it interfaces with the user can be critical factors in creating additional perceptual errors.

5. CONCLUSION

In this paper we presented a general theoretical framework to investigate the choice of eye-point location based on two metrics: minimum rendered depth and angular errors. Under the assumption that the HMD hardware is set for either near-field or far-field visualization, results of a numerical investigation show that the pupil should be chosen as the eye point if angular errors must be minimized, whereas the center of rotation should be chosen as the eye point if depth errors must be minimized. Results further show that under the best visualization condition (i.e., HMD setting, best eye point) and at 1-m near-field visualization, the maximum depth error will be 1 mm, which can be resolved at low eccentricity, yet it is well within the specification of most HMD applications. Angular errors, whether in the near or the far field, are found under the best conditions to be negligible when put in the context of the visual acuity of the human visual system.

ACKNOWLEDGMENTS

We thank Laurent Vaissie for his early assistance with this research. We also thank the reviewers for their in-depth comments about this work and their pointers to important papers in the vision literature. This research was supported by U.S. Office of Naval Research grants N00014-02-1-0261 and N00014-03-1-0677 and National Science Foundation grants IIS/ITR-0082016 and IIS/HCI-0307189.

Corresponding author Jannick Rolland can be reached at Optical Diagnostics and Applications Laboratory, School of Optics/CREOL/FPCE, University of Central Florida, Orlando, Florida 32816: E-mail, jannick @odalab.ucf.edu; phone, 407-823-6870.

REFERENCES

1. J. P. Rolland, C. Meyer, K. Arthur, and E. Rinalducci, "Methods of adjustments versus method of constant stimuli in the quantification of accuracy and precision of rendered depth in head-mounted displays," Presence Teleoperators Virtual Environ. **11**, 610–625 (2002).
2. J. E. Cutting, *Perception with an Eye for Motion* (MIT Press, Cambridge, Mass., 1986).
3. J. D. Foley and A. van Dam, *Fundamentals of Interactive Computer Graphics* (Addison-Wesley, Reading, Mass., 1984).
4. W. Robinett and J. P. Rolland, "A computational model for the stereoscopic optics of a head-mounted display," Presence Teleoperators Virtual Environ. **1**, 45–62 (1992).
5. I. P. Howard and B. J. Rogers, *Binocular Vision and Stereopsis*, No. 29 of Oxford Psychologic Series (Oxford U. Press, New York, 1995), pp. 591–593.
6. R. L. Holloway, "Registration errors in augmented reality systems," Ph.D. dissertation (University of North Carolina at Chapel Hill, Chapel Hill, N.Car., 1994) (unpublished).
7. J. P. Rolland, D. Ariely, and W. Gibson, "Towards quantifying depth and size perception in virtual environments," Presence Teleoperators Virtual Environ. **4**, 24–49 (1995).
8. J. Siderov and R. S. Harwerth, "Precision of stereoscopic depth perception from double images," Vision Res. **33**, 1553–1560 (1993).
9. D. Brewster, "On the law of visible position in single and binocular vision, and on the representation of solid figures by the union of dissimilar plane pictures on the retina," Trans. R. Soc. Edinburgh. **15**, 349–368 (1844).
10. J. P. Wann, S. Rushton, and M. Mon-Williams, "Natural problems for stereoscopic depth perception in virtual environments," Vision Res. **35**, 2731–2736 (1995).
11. K. N. Ogle and P. Boeder, "Distortion of stereoscopic spatial localization," J. Opt. Soc. Am. **38**, 723–733 (1948).
12. K. N. Ogle, "Spatial localization through binocular vision," in *The Eye* (Academic, New York, 1962), Vol. 4, pp. 409–417.
13. J. P. Rolland, "Head-mounted displays for virtual environments: the optical interface," (invited paper), in *International Lens Design Conference*, Vol. 22 of 1994 OSA Proceedings Series (Optical Society of America, Washington, D.C., 1994), pp. 329–333.
14. D. S. Goodman, "General principles of geometrical optics," in *Handbook of Optics*, Vol. 1, 2nd ed., M. Bass, ed. (McGraw-Hill, New York, 1995), pp. 1.3–1.109.
15. M. Ye, A. Bradley, L. N. Thibos, and X. Zhang, "Interocular differences in transverse chromatic aberration determine chromostereopsis for small pupils," Vision Res. **32**, 1787–1796 (1991).
16. P. Simonet and M. C. W. Campbell, "Effect of illuminance on the directions of chromostereopsis and transverse chromatic aberration observed with natural pupils," Ophthalmic Physiol. Opt. **10**, 271–279 (1990).
17. R. B. Rabbetts, ed., *Bennett and Rabbetts' Clinal Visual Optics*, 3rd ed. (Butterworth Heinemann, Oxford, UK, 1998), pp. 220–221.
18. W. S. Stiles and B. H. Crawford, "The luminous efficiency of rays entering the eye pupil at different points," Proc. R. Soc. London **112**, 428–450 (1933).
19. C. Deering, "High resolution virtual reality," Comput. Graph. **26**(2), 195–202 (1992).
20. G. A. Fry, *Geometrical optics* (Chilton book company, Philadelphia, Pa., 1969).
21. L. Vaissie and J. P. Rolland, "Eye-tracking integration in head-mounted displays," U.S. patent 6,433,760B1 (August 13, 2002).
22. J. P. Rolland, A. Yoshida, L. D. Davis, and J. H. Reif, "High-resolution inset head-mounted display," Appl. Opt. **37**, 4183–4193 (1998).
23. J. P. Rolland, M. Krueger, and A. Goon, "Multi-focal planes in head-mounted displays," Appl. Opt. **39**, 3209–3215 (2000).
24. J. P. Rolland and H. Fuchs, "Optical versus video see-through head-mounted displays," in *Fundamentals of Wearable Computers and Augmented Reality*, W. Barfield and T. Caudell, eds. (Erlbaum, Mahwah, N.J., 2001), 113–156.
25. D. B. Diner and D. H. Fender, *Human Engineering in Stereoscopic Viewing Devices* (Plenum, New York, 1993).
26. L. Davis, J. Rolland, F. Hamza-Lup, Y. Ha, J. Norfleet, B. Pettitt, and C. Imielinska, "Alice's Adventures in Wonderland: a unique technology enabling a continuum of virtual environment experiences," IEEE Comput. Graphics Appl. **23**, 10–12 (2003).
27. K. R. Boff, L. Kaufman, and J. P. Thomas, *Handbook of Perception and Human Performance* (Wiley, New York, 1986).